

Low hydrogen contents in the cores of terrestrial planets

Vincent Clesi, Mohamed Ali M.A. Bouhifd, Nathalie Bolfan-Casanova, Geeth Manthilake, Federica Schiavi, Caroline Raepsaet, Helene Bureau, Hicham Khodja, Denis Andrault

▶ **To cite this version:**

Vincent Clesi, Mohamed Ali M.A. Bouhifd, Nathalie Bolfan-Casanova, Geeth Manthilake, Federica Schiavi, et al.. Low hydrogen contents in the cores of terrestrial planets. Science Advances , 2018, 4 (3), pp.e1701876. 10.1126/sciadv.1701876 . cea-01736955

HAL Id: cea-01736955
https://cea.hal.science/cea-01736955

Submitted on 19 Mar 2018

HAL is a multi-disciplinary open access archive for the deposit and dissemination of scientific research documents, whether they are published or not. The documents may come from teaching and research institutions in France or abroad, or from public or private research centers.

L'archive ouverte pluridisciplinaire **HAL**, est destinée au dépôt et à la diffusion de documents scientifiques de niveau recherche, publiés ou non, émanant des établissements d'enseignement et de recherche français ou étrangers, des laboratoires publics ou privés.



Distributed under a Creative Commons Attribution - NonCommercial 4.0 International License

PLANETARY SCIENCE

Low hydrogen contents in the cores of terrestrial planets

Vincent Clesi,[1]* Mohamed Ali Bouhifd,[1]* Nathalie Bolfan-Casanova,[1] Geeth Manthilake,[1] Federica Schiavi,[1] Caroline Raepsaet,[2] Hélène Bureau,[3] Hicham Khodja,[2] Denis Andrault[1]

Copyright © 2018 The Authors, some rights reserved; exclusive licensee American Association for the Advancement of Science. No claim to original U.S. Government Works. Distributed under a Creative Commons Attribution NonCommercial License 4.0 (CC BY-NC).

Hydrogen has been thought to be an important light element in Earth's core due to possible siderophile behavior during core-mantle segregation. We reproduced planetary differentiation conditions using hydrogen contents of 450 to 1500 parts per million (ppm) in the silicate phase, pressures of 5 to 20 GPa, oxygen fugacity varying within IW-3.7 and IW-0.2 (0.2 to 3.7 log units lower than iron-wüstite buffer), and Fe alloys typical of planetary cores. We report hydrogen metal-silicate partition coefficients of ~2×10^{-1}, up to two orders of magnitude lower than reported previously, and indicative of lithophile behavior. Our results imply H contents of ~60 ppm in the Earth and Martian cores. A simple water budget suggests that 90% of the water initially present in planetary building blocks was lost during planetary accretion. The retained water segregated preferentially into planetary mantles.

INTRODUCTION

A solar-like atmosphere rich in H_2 and He persisted in the nebula for several million years after the onset of solar system formation (*1*), at which time Mars-sized planetary bodies had already formed (*2*). Consequently, there was sufficient time for chemical reaction between the condensed silicate rocks and hydrogen, as evidenced by primitive meteoritic material containing up to ~10 weight % (wt %) water [for example, carbonaceous chondrites (*3*)]. Unfortunately, we do not know what fraction of this water was lost during the energetic impacts between planetesimals during planetary accretion. *D*/*H* ratios show that present-day volatile elements on Earth are the result of primordial accretion from wet planetesimals (*4*, *5*). As a result, the 500- to 3000-ppm (parts per million) (*4*, *6*) and 200-ppm (*7*) water in the Earth and Martian mantles, respectively, should be mostly primordial. Thus, core-mantle segregation probably occurred in the presence of a significant amount of hydrogen.

So far, the only studies tentatively addressing hydrogen behavior during core-mantle segregation are reports of H partitioning between hydrous iron (FeH_x) and hydrous silicate, solid or molten, at high pressure (*8*–*10*). These previous results suggest that the core density deficit could be explained by a high concentration of hydrogen in the core. However, liquid water was identified in run products, implying a partial pressure of H_2O (f_{H_2O}) of several gigapascals. These experimental conditions are relevant to the determination of maximal H solubility in coexisting metal and silicate phases, but f_{H_2O} is several orders of magnitude greater than during core-mantle segregation in early Earth and Mars, which could induce major artifacts. Furthermore, the experimental conditions described in these studies are hardly transposable to continuous accretion models of mantle-core segregation in a magma ocean (*11*–*13*), which are so far the models that best describe several geochemical features, including the abundance of moderately siderophile elements in the mantle and the short time scale of core formation determined by Hf/W chronometry (*14*).

[1]Laboratoire Magmas et Volcans, Université Clermont Auvergne, CNRS UMR 6524, Observatoire de Physique du Globe de Clermont Ferrand–Institut de Recherche pour le Développement, Campus Universitaire des Cézeaux, 6 Avenue Blaise Pascal, 63178 Aubière Cedex, France. [2]Laboratoire d'Etude des Eléments Légers, Nanosciences et Innovation pour les Matériaux, la Biomédecine et l'Énergie, Commissariat à l'Energie Atomique et aux Energies Alternatives (CEA), CNRS, Université Paris-Saclay, CEA Saclay, 91191 Gif sur Yvette Cedex, France. [3]Institut de Minéralogie et de Physique de la Matière et de Cosmochimie, Sorbonne Universités, UMR CNRS-UPMC 7590, 4 place Jussieu, 75252 Paris, France.
*Corresponding author. Email: A.Bouhifd@opgc.univ-bpclermont.fr (M.A.B.); v.clesi@opgc.univ-bpclermont.fr (V.C.)

Experimental procedure

In line with recent models proposed for the accretion of Earth and Mars (*11*, *12*), we investigated hydrogen partitioning between a molten CI chondritic-type mantle and a liquid Fe alloy (Table 1) at pressures and temperatures of up to 20 GPa and ~2500 K, respectively, using a large-volume press apparatus. In the Fe alloy, we included all elements primary to planetary cores (Fe, Ni, Co, C, Si, and S) because incorporation of hydrogen into the metal can be sensitive to even trace amounts of those elements [see the study of *Lob et al.* (*15*) and references therein]. The bulk H_2O content in the sample was adjusted between 450 ppm and 1.5 wt % by addition of an appropriate amount of $Al(OH)_3$. Oxygen fugacity (f_{O_2}) was adjusted between 3.5 and 0.2 log units below the iron-wüstite buffer (IW-3.5 to IW-0.2) by addition of Si to the metal (Table 1) (*16*). This f_{O_2} range corresponds to recent models of multistage core-mantle differentiation, based on heterogeneous accretion of Earth from an initial 60 to 70 wt % of reduced material, followed by a final 30 to 40 wt % of more oxidized material (*11*, *12*). After synthesis at high pressure and temperature, microstructures of run products were examined by scanning electron microscopy (Fig. 1). Major and trace elements in each phase were analyzed by electron microprobe and laser ablation inductively coupled plasma mass spectroscopy (LA-ICPMS), respectively [see tables S1 and S2, Supplementary Materials, and the study of Clesi *et al.* (*16*)].

RESULTS

Possibility of quenching hydrogen in the metallic phase

The quenched molten Fe-rich metals recovered from our experiments show "smooth" surfaces after polishing and no bubbles at the surface (Fig. 1). Also, the mass balance of water in our run products suggests no loss of hydrogen. This apparent contradiction with the results of Okuchi (*8*) and Iizuka-Oku *et al.* (*10*), where hydrogen was lost after quenching, can be explained by the difference in hydrogen fugacity during the experiments. In previous studies, high hydrogen fugacities in the range of gigapascals (10^9 Pa) led to the hydrogen saturation of the metallic phase, producing H bubbles upon decompression. Here, we avoided the H saturation in the Fe-rich alloys by the addition of only 450 to 1500 ppm of hydrogen. Furthermore, the loss of H from the metal phase during quenching by H diffusion (Fick's law) without the formation of bubbles is also very unlikely. The low value (10^{-10} to 10^{-9} m^2/s) of the diffusion coefficient of hydrogen in liquid alloys at high temperature (*17*) would yield

Downloaded from http://advances.sciencemag.org/ on March 19, 2018

Table 1. Experimental conditions and compositions of recovered samples. Detailed compositions of the silicate and metal phases in the recovered samples are given in tables S1 and S2, respectively. n.d., not detected.

Sample	T (K)	P (GPa)	Log fo_2^*	Ni^{met} (wt %)	Co^{met} (wt %)	Si^{met} (wt %)	C^{met} (wt %)	S^{met} (wt %)
V1	2245	5	−1.37	8.7	4.43	0.07	4.21	0
W8	2125	5	−1.04	8.37	4.21	0.01	5.48	0
W16	2020	5	−1.45	9.59	4.17	0.014	4.86	0
W12	2375	10	−0.95	9.37	4.35	0.018	5.69	0
W19	2125	10	−0.68	10.2	4.13	0.012	5.74	0
W34	2700	21	−1.21	7.9	3.93	0.03	7.50	0
SiW1	2240	5	−3.75	8.06	3.56	8.68	2.99	0
SiW8	2775	20	−3.54	8.7	3.26	5.1	5.44	0
SW3	2325	10	−0.20	3.71	n.d.	0.01	3.51	27.22

*Oxygen fugacity is given relative to the iron-wüstite buffer (*16*).

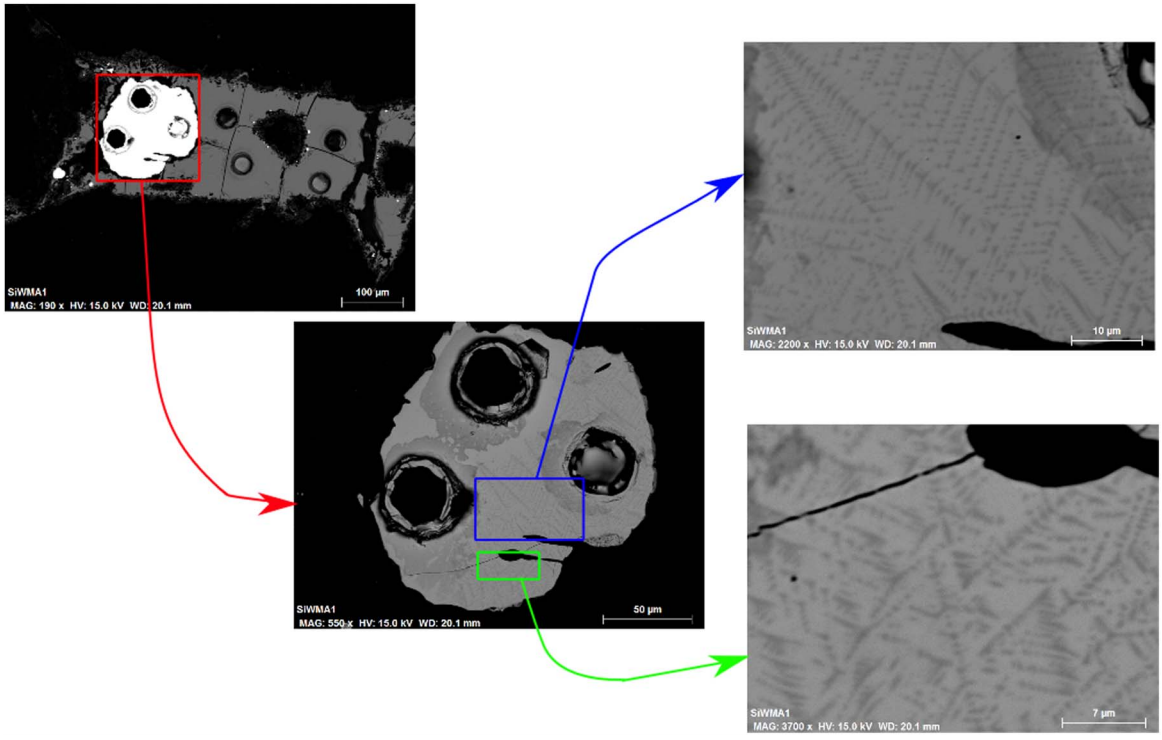


Fig. 1. Backscattered electron micrograph showing the texture of quenched metal for sample SiW1. Left to right: The images zoom in from full sample to the bulk metallic phase and to metallic quench structures of Fe-Si darker than the Fe-Ni alloy surrounding it. The holes are LA-ICPMS pits made during the analysis of composition. The absence of hydrogen bubbles in the metallic phase is observed in all our samples. It evidences no exsolution of the hydrogen from the metal. This contrast of texture compared to the study of Okuchi (*8*) is due to the low hydrogen content in our bulk sample, preventing the metal saturation in hydrogen and therefore the loss of hydrogen during decompression.

time of diffusion of several hours for the metal to lose hydrogen, as observed by Iizuka-Oku *et al.* (*10*). Depuydt and Parlee (*18*) have also determined the activation energy of hydrogen to be several kilojoules per mole, thus preventing hydrogen from exsolving from the quenched metal at room temperature after quenching and polishing.

Hydrogen partitioning between molten silicate and metallic liquid

Among other methods used, elastic recoil detection analysis (ERDA; see the Supplementary Materials, Fig. 2, and fig. S1) provided the most quantitative water content measurements in coexisting metal and silicate phases, and those results are used henceforth to address

Downloaded from http://advances.sciencemag.org/ on March 19, 2018

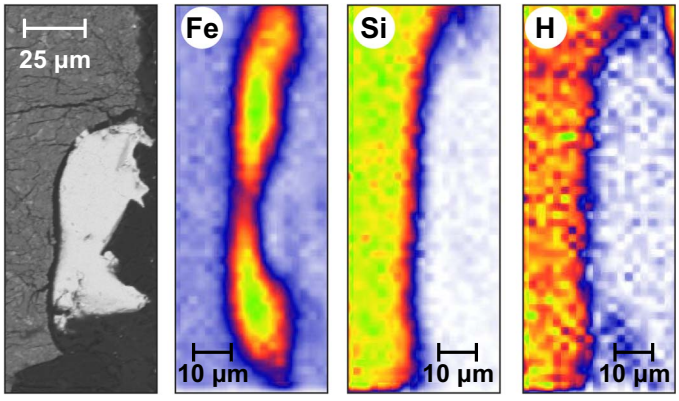


Fig. 2. Backscattered electron photomicrograph and chemical analysis of sample W34. Left to right: Images are the backscattered electron (BSE) photomicrograph, Fe and Si contents measured by x-ray fluorescence, and H content measured by ERDA. Color scales range from 0 (minimum, white) to 522 (maximum, green), 0 to 768, and 0 to 53, for increasing abundances of Si, Fe, and hydrogen, respectively. Preliminary chemical maps were first acquired using particle-induced x-ray emission (PIXE) to facilitate the selection of specific regions of metal and silicate, where ERDA was then performed. The increased hydrogen abundance in the silicate suggests its lithophile behavior. The elongated shape observed in the chemical maps, compared to the BSE photomicrograph, is due to a spatial resolution four times lower in the vertical direction of PIXE and ERDA acquisitions.

Table 2. Hydrogen concentrations in coexisting silicate and metal phases. We also report the metal-silicate partition coefficient of hydrogen ($D_H^{met\text{-}sil}$). Numbers in parentheses are the associated 1σ uncertainties. All values are obtained by ERDA, except for sample W12.

Sample	H in silicate (ppm)	H in metal (ppm)	D_H
V1	402 (100)	19.5 (7.9)	0.048 (32)
W16	452 (113)	75 (17)	0.166 (81)
W8	665 (166)	120 (30)	0.181 (91)
W12	353* (88)	59 (12)	0.167 (77)
W19	1234 (309)	63.4 (5.5)	0.051 (17)
W34	752 (188)	254 (53)	0.34 (15)
SiW1	465 (116)	18.9 (7.8)	0.041 (27)
SiW8	678 (170)	524 (89)	0.77 (32)
SW3	541 (135)	23.6 (1.9)	0.044 (14)

*Value in the silicate phase determined using the Al-proxy calculation [see the Supplementary Materials and the study of Clesi (*16*)] because of a lack of ERDA measurements.

metal-silicate H partitioning. The spatial resolution on the sample was ~3 × 12 μm^2. We achieved an H detection limit of ~30 ppm by weight H_2O (*19*, *20*) in the silicate phase, and our ERDA results (Table 2) are in good agreement with those determined using the Al-proxy and Raman analyses [see the Supplementary Materials, fig. S2, and the study of Clesi *et al.* (*16*)]. Several studies have validated the use of ERDA for the determination of H content in minerals, including a recent systematic comparison with nanoscale secondary ion mass spectrometry results (*21*). For metals, the capability of ERDA for H content determination is unique, providing a detection limit of ~50 ppm by weight H_2O (see the Supplementary Materials).

Hydrogen partition coefficients between molten silicate and metallic liquid ($D_H^{met\text{-}sil} = [H]^{Metal\text{-}liquid}/[H]^{Silicate\text{-}liquid}$) in all our samples are between 4×10^{-2} and 8×10^{-1}, with an average value of ~2×10^{-1} (Fig. 3 and Table 2). Our partition coefficient values represent lithophile behavior for H across a wide range of fO_2, *P*, and *T* conditions typical of planetary core formation. These $D_H^{met\text{-}sil}$ values are two to three orders of magnitude lower than those reported in previous studies (*8*, *9*), likely because of the extremely high fH_2O values used previously, which, as discussed above, are not relevant to planetary formation.

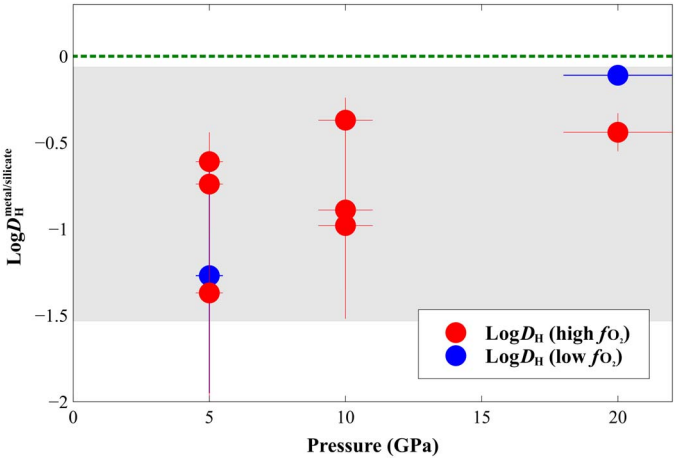


Fig. 3. Hydrogen partitioning between metal and silicate (log$D_H^{met\text{-}sil}$) as a function of experimental pressure. Red and blue circles represent experiments performed at oxygen fugacities above IW-2 and below IW-3.5, respectively. The green dashed line at log$D_H^{met\text{-}sil}$ = 0 indicates the limit between lithophile (below) and siderophile behavior (above). The gray area encompasses the range of D_H values determined from our experiments, all of which indicate lithophile behavior.

DISCUSSION

Thermodynamics of hydrogen partitioning between metal and silicate

To describe our experimental results, the thermodynamical model should account for the dependence of the H content of Fe-rich alloys ($[H]_{metal}$) with the water content of the silicate as well as the dependence of H partitioning on pressure, temperature, and oxygen fugacity. Our experiments show that the dependence on the fO_2 is negligible (Fig. 3), so we consider that no parameter is needed to account for the fO_2 variation during planetary accretion.

H_2 is likely a significant hydrous species in silicate liquids under reducing conditions applicable to planetary and deep Earth magmas (*22*). In addition, the equilibrium of redox potential in nature is dominated by H_2 transfer at a rate controlled by both H_2 solubility and diffusion (*23*). For this, the following formalism was used on the basis of the dilute solution theory (*15*)

$$\frac{1}{2}[H_2]_{silicate} \rightarrow H_{metal} \quad (1)$$

Downloaded from http://advances.sciencemag.org/ on March 19, 2018

$$[H]_{metal} = \frac{K_H}{f_H} \times \sqrt{P_{H2}} \quad (2)$$

where K_H is the solubility constant of Eq. 1, f_H is the activity coefficient of hydrogen in metal, and P_{H2} is the partial pressure of H_2. Because the exact value of P_{H2} is difficult to determine, we based our model on the H_2 concentration (in mole percent) in the silicate melt (X_{H2}), assuming a linear evolution of X_{H2} with experimental P_{H2}. Therefore, we estimate the hydrogen fugacity in the experiment by calculating the molar concentration of H_2 in the melt. Because we do not have any information on the activity coefficient of H_2 in high-pressure silicate melts, we considered it to be equal to 1. For the metal-silicate partitioning experiments [this study and from the studies of Okuchi (*8*) and Iizuka-Oku *et al.* (*10*)], we considered that $P_{H2} = a_{H2} = X_{H2}$. When considering 1-bar experiments (*16*), because the partial pressure is well known, we do not use the latter assumption.

The activity coefficient of hydrogen in metal depends on the concentration of each element i in the metal X^i (wt %) and the interaction parameters between H and each element (ε_H^i) (table S3)

$$\log f_H = \Sigma \varepsilon_H^i \times X^i \quad (3)$$

Finally, K_H is a function of pressure and temperature

$$\log K_H = \frac{A}{T(K)} + \frac{B \times P(GPa)}{T(K)} + C \quad (4)$$

where A, B, and C are adjusted to minimize the difference between theoretical and experimental K_H values, using all existing experimental data on H incorporation into Fe-rich alloy liquids (see the Supplementary Materials and fig. S4). We performed the adjustment in two steps: We first refined the temperature dependence (A) using the large data set available at 1 bar (*15*) and then refined B and C using all available data. The best fit yields $A = -1815 \pm 270$ K, $B = 231 \pm 38$ K·GPa^{-1}, and $C = 2.64 \pm 0.48$. This empirical thermodynamical model predicts H concentration in coexisting metal and silicate liquids at pressures and temperatures relevant to core-mantle segregation with an accuracy of ±50%. As shown in fig. S3, this model fit our data, high-pressure data (*8*, *10*), and 1-bar experiments (*15*).

Implications for hydrogen contents in planetary cores and mantles

To investigate the behavior of water during core-mantle segregation on Earth and Mars, the primordial bulk water contents must be defined. In our previous study (*16*), we showed that the maximum bulk water concentrations should be 1.2 to 1.8 wt % for Earth and 2.5 to 3.5 wt % for Mars. Our calculation accounts for the different compositions of the two planetary cores: both are Fe alloys, with 8.7 wt % Ni, 12 wt % Si, and 2 wt % S for Earth and 8.5 wt % Ni, 0.05 wt % Si, and 15 wt % S for Mars. As accretion proceeded, the composition of the planetary building blocks probably changed from EH to more oxidized bodies at mass fractions of 85 and 75% of Earth and Mars, respectively (*11*). If we assume that the more oxidized bodies are similar to CI chondrites, the late-stage compositional change to CI chondrite induced a significant increase in the H content of the cores, reaching maximum core H concentrations of 64 ppm (Earth) and 57 ppm (Mars) by the end of planetary accretion (Fig. 4). These low H concentrations are in good agreement with the very low H contents of metallic meteorites (9 parts per billion), which are considered to be representative of the cores of primitive, relatively small planetesimals (*24*). Independent isotopic constraints refute significant hydrogen incorporation into the core, because

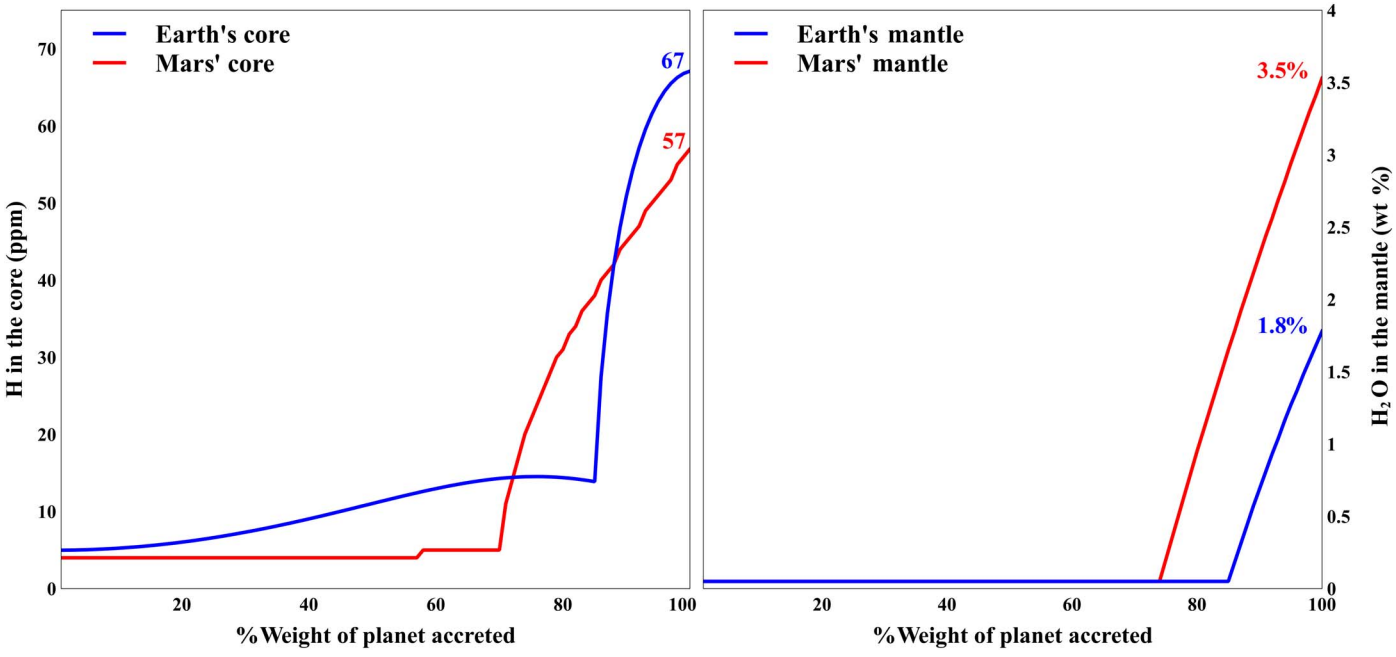


Fig. 4. Core hydrogen contents (in ppm, left) and mantle H_2O contents (in wt %, right) during the course of accretion of Earth and Mars. The base model considers heterogeneous planetary accretion, first of EH chondrites (to 85 and 75% accretion of Earth and Mars, respectively), and later of CI chondrites (the final 15 and 25% of Earth and Mars, respectively). Planetary building block compositions are detailed elsewhere (*11*, *12*, *16*). Low H content in planetary cores is attributed to the presence of Si (fig. S5).

Downloaded from http://advances.sciencemag.org/ on March 19, 2018

of the relatively high δ^{57}Fe value of Earth's mantle (*25*). We note that the relatively low hydrogen concentrations in Fe alloys are partially due to significant Si and S contents, which disfavor H incorporation into the cores (Eq. 3 and tables S2 and S3).

Because of the limited incorporation of hydrogen into Earth's core, a relatively high water content in the magma ocean could have major implications. First, hydrogen is likely to be exsolved in the residual melt upon crystallization of the magma ocean (*26*, *27*). At one point, the melt could become saturated in H_2 and will be released in the atmosphere [see the study of Hirschmann *et al.* (*22*) and references therein]. This effect could have also induced major changes of the upper mantle oxidation state (*28*).

MATERIALS AND METHODS

Sample compositions

Starting materials consisted of 50:50 wt % mixtures of a synthetic silicate CI chondrite model composition and Fe-rich alloys. The composition of the silicate fraction is 49.6 wt % SiO_2, 35.1 wt % MgO, 8.5 wt % FeO, 3.5 wt % Al_2O_3, and 3.3 wt % CaO, similar to that in a previous study (*29*). We added up to 0.5 wt % V_2O_3, Cr_2O_3, and MnO. The Fe-rich alloys were mixed from metallic powders, with a basic composition of 85 wt % Fe, 10 wt % Ni, and 5 wt % Co. Then, the experimental fO_2 was monitored between IW-2 and IW-5 by addition of up to 10 wt % Si to the metal. In run products, these fO_2 conditions correspond to FeO contents in the silicate phase ranging from ~0.2 wt % (low fO_2) to ~6.5 wt % (high fO_2). In some cases, FeS was added to the starting material, reaching a maximum S content of 27 wt % in the metal (all compositions reported in tables S2 and S3). Finally, the bulk water content was controlled by adding $Al(OH)_3$ to the sample mixture. This phase completely dehydrated into water and corundum at high pressure and temperature.

Choice of capsule

We performed test experiments to check water loss in our samples at 1 to 3 GPa and 1623 to 1873 K using a piston-cylinder apparatus [experimental methods are reported elsewhere (*30*)]. We used either a single graphite capsule or double capsules with inner $Au_{80}Pd_{20}$ (or graphite above 1873 K) and outer Pt capsules. Experimental durations for these tests were between 2 and 20 min. In both setups and at all tested durations, we found good agreement between water contents measured by Fourier transform infrared spectroscopy (FTIR) in the quenched silicate melt and those estimated from the Al-proxy [based on the amount of $Al(OH)_3$ added to the starting material; see the study of Clesi *et al.* (*16*)]. Thus, a single graphite capsule was used for all further experiments, and durations were limited to ~2 min. Graphite capsules have the added advantage of stability at the extremely high temperatures relevant to magma oceans on terrestrial planets such as Earth and Mars (*31*).

Semiquantitative analysis of carbon content in the quenched Fe alloys found an increase from ~3 to ~7 wt % C with increasing pressure (table S2). This trend is in good agreement with previous studies on metal-silicate partitioning, as well as the thermodynamics of carbon solubility in metallic alloys [see the studies of Dasgupta and Walker (*32*), Wood (*33*), and Bouchard and Bale (*34*) and references therein]. The presence of C in the Fe alloys is taken into account by the thermodynamical model developed in this study (table S3).

Sample synthesis at high pressure and temperature

Experiments were conducted using the 1500-ton multi-anvil press at the Laboratoire Magmas et Volcans. Experimental conditions and pressure calibrations were similar to those described previously (*35*). Experiments at 5 to 10 and 15 to 20 GPa were performed using the 14/8 (MgO-doped octahedral of 14-mm edges and WC anvils with 8-mm truncation) and 10/4 assemblies, respectively. Samples were first compressed to the desired pressure before progressive heating to the target temperature. Stepped $LaCrO_3$ furnaces were used to reduce the temperature gradient in the axial direction. The sample temperature was monitored using a $W_{95}Re_5$-$W_{74}Re_{26}$ (C type) thermocouple, whose junction was in contact with the top of the graphite capsule. No pressure correction was made for the thermocouple electromotive force, which, in addition to the variations of temperatures during experiments, yields an uncertainty of ±100 K. In the event of thermocouple loss, the heater power was used to estimate the sample temperature. Samples were held at the maximum temperature for 1 to 2 min, which is sufficient to achieve equilibrium between silicate and metallic liquids [see the study of Bouhifd *et al.* (*29*) and references therein]. Finally, samples were quenched at ~100 K/s by shutting off the power to the heater.

The recovered octahedral pressure medium was mounted in epoxy, mirror-polished, and carbon-coated under vacuum. At experimental pressures above 10 GPa, the graphite capsules transformed into diamond, thus requiring diamond-based polishing tools. To avoid atmospheric contamination, samples were stored in a dry furnace at 50°C.

SUPPLEMENTARY MATERIALS

Supplementary material for this article is available at http://advances.sciencemag.org/cgi/content/full/4/3/e1701876/DC1

Water content determination

Thermodynamical model refinement for H metal-silicate partitioning

fig. S1. ERDA signal in quenched silicate melt (left) and metal (right) of sample SiW1.

fig. S2. Comparison of H contents measured by ERDA and other techniques for determination of H content in the silicate phase.

fig. S3. Comparison between experimental and theoretical K_H values.

fig. S4. Example of water content determination using Raman spectroscopy.

fig. S5. Evolution of the core compositions of Earth (left) and Mars (right) during the course of planetary accretion.

table S1. Composition of quenched silicate melts.

table S2. Composition of metals.

table S3. Interaction parameters between hydrogen and each element *i* present in the metal [from (*15*)].

References (*36*–*40*)

REFERENCES AND NOTES

1. F. A. Podosek, P. Cassen, Theoretical, observational, and isotopic estimates of the lifetime of the solar nebula. *Meteoritics* **29**, 6–25 (1994).
2. N. Dauphas, A. Pourmand, Hf–W–Th evidence for rapid growth of Mars and its status as a planetary embryo. *Nature* **473**, 489–492 (2011).
3. A. R. Sarafian, S. G. Nielsen, H. R. Marschall, F. M. McCubbin, B. D. Monteleone, Early accretion of water in the inner solar system from a carbonaceous chondrite–like source. *Science* **346**, 623–626 (2014).
4. B. Marty, The origins and concentrations of water, carbon, nitrogen and noble gases on Earth. *Earth Planet. Sci. Lett.* **313–314**, 56–66 (2012).
5. A. N. Halliday, The origins of volatiles in the terrestrial planets. *Geochim. Cosmochim. Acta* **105**, 146–171 (2013).
6. A. Férot, N. Bolfan-Casanova, Water storage capacity in olivine and pyroxene to 14 GPa: Implications for the water content of the Earth's upper mantle and nature of seismic discontinuities. *Earth Planet. Sci. Lett.* **349–350**, 218–230 (2012).
7. G. J. Taylor, The bulk composition of Mars. *Chem. Erde Geochem.* **73**, 401–420 (2013).
8. T. Okuchi, Hydrogen partitioning into molten iron at high pressure: Implications for Earth's Core. *Science* **278**, 1781–1784 (1997).

Downloaded from http://advances.sciencemag.org/ on March 19, 2018

9. Y. Fukai, T. Suzuki, Iron-water reaction under high pressure and its implication in the evolution of the Earth. *J. Geophys. Res. Solid Earth Planets* **91**, 9222–9230 (1986).
10. R. Iizuka-Oku, T. Yagi, H. Gotou, T. Okuchi, T. Hattori, A. Sano-Furukawa, Hydrogenation of iron in the early stage of Earth's evolution. *Nat. Commun.* **8**, 14096 (2017).
11. D. C. Rubie, S. A. Jacobson, A. Morbidelli, D. P. O'Brien, E. D. Young, J. de Vries, F. Nimmo, H. Palme, D. J. Frost, Accretion and differentiation of the terrestrial planets with implications for the compositions of early-formed Solar System bodies and accretion of water. *Icarus* **248**, 89–108 (2015).
12. J. Wade, B. J. Wood, Core formation and the oxidation state of the Earth. *Earth Planet. Sci. Lett.* **236**, 78–95 (2005).
13. M. A. Bouhifd, V. Clesi, A. Boujibar, N. Bolfan-Casanova, C. Cartier, T. Hammouda, M. Boyet, G. Manthilake, J. Monteux, D. Andrault, Silicate melts during Earth's core formation. *Chem. Geol.* **461**, 128–139 (2017).
14. T. Kleine, M. Touboul, B. Bourdon, F. Nimmo, K. Mezger, H. Palme, S. B. Jacobsen, Q.-Z. Yin, A. N. Halliday, Hf–W chronology of the accretion and early evolution of asteroids and terrestrial planets. *Geochim. Cosmochim. Acta* **73**, 5150–5188 (2009).
15. A. Lob, D. Senk, B. Hallstedt, Determination of hydrogen solubility in Fe–Mn–C melts. *Steel Res. Int.* **82**, 108–113 (2011).
16. V. Clesi, M. A. Bouhifd, N. Bolfan-Casanova, G. Manthilake, A. Fabbrizio, D. Andrault, Effect of H_2O on metal–silicate partitioning of Ni, Co, V, Cr, Mn and Fe: Implications for the oxidation state of the Earth and Mars. *Geochim. Cosmochim. Acta* **192**, 97–121 (2016).
17. W. Beck, J. O. M. Bockris, M. A. Genshaw, P. K. Subramanyan, Diffusivity and solubility of hydrogen as a function of composition in Fe-Ni alloys. *Metall. Trans.* **2**, 883–888 (1971).
18. P. J. Depuydt, N. A. D. Parlee, The diffusion of hydrogen in liquid iron alloys. *Metall. Mater. Trans. B* **3**, 529–536 (1972).
19. A. C. Withers, H. Bureau, C. Raepsaet, M. M. Hirschmann, Calibration of infrared spectroscopy by elastic recoil detection analysis of H in synthetic olivine. *Chem. Geol.* **334**, 92–98 (2012).
20. H. Bureau, C. Raepsaet, H. Khodja, A. Carraro, C. Aubaud, Determination of hydrogen content in geological samples using elastic recoil detection analysis (ERDA). *Geochim. Cosmochim. Acta* **73**, 3311–3322 (2009).
21. D. Novella, D. J. Frost, E. H. Hauri, H. Bureau, C. Raepsaet, M. Roberge, The distribution of H_2O between silicate melt and nominally anhydrous peridotite and the onset of hydrous melting in the deep upper mantle. *Earth Planet. Sci. Lett.* **400**, 1–13 (2014).
22. M. M. Hirschmann, A. C. Withers, P. Ardia, N. T. Foley, Solubility of molecular hydrogen in silicate melts and consequences for volatile evolution of terrestrial planets. *Earth Planet. Sci. Lett.* **345–348**, 38–48 (2012).
23. F. Gaillard, B. Schmidt, S. Mackwell, C. McCammon, Rate of hydrogen–iron redox exchange in silicate melts and glasses. *Geochim. Cosmochim. Acta* **67**, 2427–2441 (2003).
24. C. Defouilloy, R. Duhamel, F. Robert, Ion microprobe determination of hydrogen concentration and isotopic ratio in extraterrestrial metallic alloys. *Geostand. Geoanal. Res.* **37**, 417–427 (2013).
25. A. Shahar, E. A. Schauble, R. Caracas, A. E. Gleason, M. M. Reagan, Y. Xiao, J. Shu, W. Mao, Pressure-dependent isotopic composition of iron alloys. *Science* **352**, 580–582 (2016).
26. M. M. Hirschmann, T. Tenner, C. Aubaud, A. C. Withers, Dehydration melting of nominally anhydrous mantle: The primacy of partitioning. *Phys. Earth Planet. In.* **176**, 54–68 (2009).
27. G. Hirth, D. L. Kohlstedt, Water in the oceanic upper mantle: Implications for rheology, melt extraction and the evolution of the lithosphere. *Earth Planet. Sci. Lett.* **144**, 93–108 (1996).
28. Z. D. Sharp, F. M. McCubbin, C. K. Shearer, A hydrogen-based oxidation mechanism relevant to planetary formation. *Earth Planet. Sci. Lett.* **380**, 88–97 (2013).
29. M. A. Bouhifd, M. Boyet, C. Cartier, T. Hammouda, N. Bolfan-Casanova, J. L. Devidal, D. Andrault, Superchondritic Sm/Nd ratio of the Earth: Impact of Earth's core formation. *Earth Planet. Sci. Lett.* **413**, 158–166 (2015).
30. A. Fabbrizio, M. A. Bouhifd, D. Andrault, N. Bolfan-Casanova, G. Manthilake, D. Laporte, Argon behavior in basaltic melts in presence of a mixed H_2O-CO_2 fluid at upper mantle conditions. *Chem. Geol.* **448**, 100–109 (2017).
31. Y. Li, R. Dasgupta, K. Tsuno, The effects of sulfur, silicon, water, and oxygen fugacity on carbon solubility and partitioning in Fe-rich alloy and silicate melt systems at 3 GPa and 1600°C: Implications for core–mantle differentiation and degassing of magma oceans and reduced planetary mantles. *Earth Planet. Sci. Lett.* **415**, 54–66 (2015).
32. R. Dasgupta, D. Walker, Carbon solubility in core melts in a shallow magma ocean environment and distribution of carbon between the Earth's core and the mantle. *Geochim. Cosmochim. Acta* **72**, 4627–4641 (2008).
33. B. J. Wood, Carbon in the core. *Earth Planet. Sci. Lett.* **117**, 593–607 (1993).
34. D. Bouchard, C. W. Bale, Simultaneous optimization of thermochemical data for liquid iron alloys containing C, N, Ti, Si, Mn, S, and P. *Metall. Mater. Trans. B* **26**, 467–484 (1995).
35. A. Boujibar, D. Andrault, M. A. Bouhifd, N. Bolfan-Casanova, J.-L. Devidal, N. Trcera, Metal–silicate partitioning of sulfur, new experimental and thermodynamical constraints on planetary accretion. *Earth Planet. Sci. Lett.* **391**, 42–54 (2014).
36. N. Bolfan-Casanova, G. Montagnac, B. Reynard, Measurement of water contents in olivine using Raman spectroscopy. *Am. Mineral.* **99**, 149–156 (2014).
37. E. Médard, T. L. Grove, The effect of H_2O on the olivine liquidus of basaltic melts: Experiments and thermodynamic models. *Contrib. Mineral. Petrol.* **155**, 417–432 (2008).
38. M. Weinstein, J. F. Elliott, Solubility of hydrogen in liquid iron alloys. *Trans. Met. Soc. AIME* **227**, 382–393 (1963).
39. R. G. Blossey, R. D. Pehlke, Solubility of hydrogen in liquid Fe-Co-Ni alloys. *Metall. Trans.* **2**, 3157–3161 (1971).
40. W. M. Boorstein, R. D. Pehlke, Measurement of hydrogen solubility in liquid iron alloys employing a constant volume technique. *Metall. Trans.* **5**, 399–405 (1974).

Acknowledgments: We would like to thank G. Gaetani, the editor, and two anonymous reviewers who helped us to improve our manuscript. We would also like to thank M. Boyet for many discussions about Earth's evolution. **Funding:** This study was supported by CNRS-INSU (Institut National des Sciences de l'Univers) (program: Programme National de Planétologie), Agence Nationale de la Recherche (ANR) (project: OxyDeep), ANR (project: HYDEEP), the French Government Laboratory of Excellence initiative no. ANR-10-LABX-0006, the Région Auvergne, and the European Regional Development Fund. This is Laboratory of Excellence ClerVolc contribution number 285. The multi-anvil apparatus of Laboratoire Magmas et Volcans is financially supported by the CNRS (Instrument National de l'INSU).
Author contributions: V.C. and M.A.B. initiated the project. V.C. and G.M. performed the high-pressure experiments. V.C., F.S., and N.B.-C. performed the FTIR and Raman analyses. V.C., M.A.B., C.R., H.K., H.B., and N.B.-C. performed the ERDA analyses. V.C., M.A.B., and D.A. wrote the manuscript before all authors commented on it. **Competing interests:** The authors declare that they have no competing interests. **Data and materials availability:** All data needed to evaluate the conclusions in the paper are present in the paper and/or the Supplementary Materials. Additional data related to this paper may be requested from M.A.B. (A.Bouhifd@opgc.univ-bpclermont.fr) or V.C. (v.clesi@opgc.univ-bpclermont.fr).

Submitted 1 June 2017
Accepted 6 February 2018
Published 14 March 2018
10.1126/sciadv.1701876

Citation: V. Clesi, M. A. Bouhifd, N. Bolfan-Casanova, G. Manthilake, F. Schiavi, C. Raepsaet, H. Bureau, H. Khodja, D. Andrault, Low hydrogen contents in the cores of terrestrial planets. *Sci. Adv.* **4**, e1701876 (2018).

Downloaded from http://advances.sciencemag.org/ on March 19, 2018

Science Advances

Low hydrogen contents in the cores of terrestrial planets

Vincent Clesi, Mohamed Ali Bouhifd, Nathalie Bolfan-Casanova, Geeth Manthilake, Federica Schiavi, Caroline Raepsaet, Hélène Bureau, Hicham Khodja and Denis Andrault

Sci Adv **4** (3), e1701876.
DOI: 10.1126/sciadv.1701876

ARTICLE TOOLS http://advances.sciencemag.org/content/4/3/e1701876

SUPPLEMENTARY MATERIALS http://advances.sciencemag.org/content/suppl/2018/03/12/4.3.e1701876.DC1

REFERENCES This article cites 40 articles, 4 of which you can access for free
http://advances.sciencemag.org/content/4/3/e1701876#BIBL

PERMISSIONS http://www.sciencemag.org/help/reprints-and-permissions

Use of this article is subject to the Terms of Service

Science Advances (ISSN 2375-2548) is published by the American Association for the Advancement of Science, 1200 New York Avenue NW, Washington, DC 20005. 2017 © The Authors, some rights reserved; exclusive licensee American Association for the Advancement of Science. No claim to original U.S. Government Works. The title *Science Advances* is a registered trademark of AAAS.

Downloaded from http://advances.sciencemag.org/ on March 19, 2018